Nature of Ricepiles (An Oslo Model Investigation)

February 16, 2020
Shaun Fendi Gan
CID: 01331868
(Word Count: 2500 excl. abstract)

Abstract—**Ricepiles were investigated using the Oslo Model as an example of a system with self-organised criticality, where the model's characteristics were analysed. Key results include: $a_0 = 1.737$ and $\omega_1 = 0.548$ for height scaling using chi-square minimisation. $D = 2.2149$ and $\tau_s = 1.5549$ for avalanche size scaling from moment analysis. Relationships of $h \propto t^{0.506}$ and $\sigma_h \propto L^{0.253}$ where found. Data collapses for height, height probability and avalanche size probability were completed, where the latter required log-binning. Scaling corrections were investigated for height, cross-over time, standard deviation of height and moments of avalanche size. Sites were found to tend to identical, but not independent behaviour. Additional scaling correction constants were found for avalanche size moments, indicating possible power law dependencies on k.**

I. INTRODUCTION

COMPLEXITY is the study of nature, where systems exist in non-equilibria conditions. Internal energy enters and leaves the system over time. These kinds of systems manifest themselves at all scales, such as in earthquakes, in the weather, and in the human body. This field of study allows us to draw intrinsic characteristics about a certain subsets of these systems, hopefully to develop a deeper understanding of nature and its processes.

In this project, toppling ricepiles were simulated using the Oslo model. The Oslo model introduces randomness in slope thresholds that imitate spatial and temporal fluctuations, causing it to be more realistic compared to the BTW model [1].

The Oslo model efficiency was improved by only checking adjacent slopes to the toppling site against their thresholds, compared to checking all sites. Object-Oriented-Programming was used in this project, so that each Oslo model of size L would be represented as a single object.

II. TASKS AND RESULTS

Results of each task are displayed and described chronologically in the following sections. Terminology used in the section below are summarised as:

- z_i : slope at a site i
- z_{th} : slope threshold
- L : system size
- p : probability of a slope threshold
- t : time or number of grains added

A. Implementation of the Oslo Model (Tests)

Firstly, the expected height at site i=1 was found from taking the average height of the pile, driven 1 million times after cross-over. The average height of the pile was found as

- 26.53 for L = 16 (0.12% from true value)
- 53.88 for L = 32 (-0.03% from true value)

where the % difference comes from fluctuations due to random thresholds. Rounding the estimates to 1 d.p. produces the desired values.

Secondly, for simple values of p where $p = 1$ for $z_{th} = 1$ and $p = 0$ for $z_{th} = 2$, we expect the model to reduce to a 1D-BTW model, where only one threshold slope is available. This should manifest as a simple staircase at all times, and was achieved as shown in Fig. 1.
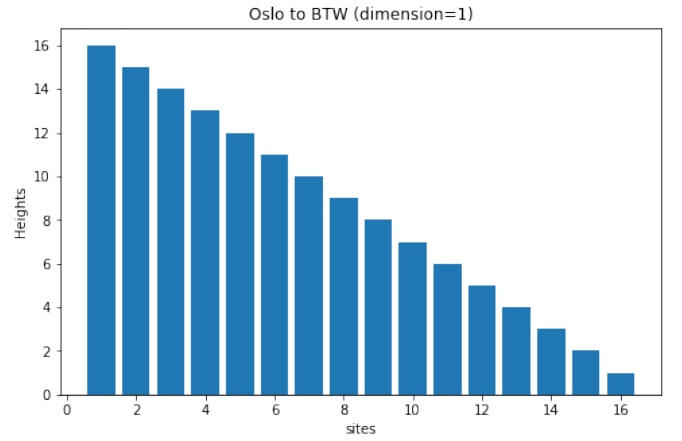

Fig. 1. Oslo model reduces to BTW model in 1D, when the probability of $z_{th} = 1$ is set to $p = 1$. This gives a characteristic staircase distribution at all times as seen above.

Thirdly, the number of recurrent configurations were found for $L = 2$ and 4. The expected number of recurrent configurations N_R is found by

$$N_{\mathcal{R}} = \frac{1}{\sqrt{5}} \left(\phi(1 + \phi)^L + \frac{1}{\phi(1 + \phi)^L} \right) \propto (1 + \phi)^L \quad (1)$$

where ϕ is the golden mean. $N_R = 5$ and $N_R = 34$ were expected respectively for $L = 2, 4$ [1].

N_R was found by counting the unique configurations of z after cross-over. The theoretical values for N_R were achieved and can be seen in the code. For $L \geq 4$ the number of transient configurations varied from run to run, as not all configurations would occur when approaching the steady state due to random thresholds.

B. Height of the Pile $h(t; L)$

Sizes of $L = [4, 8, 16, 32, 64, 128, 256, 512]$ were used for the remaining tasks, these systems were driven one million times.

2a) Heights of the pile were plotted at all times. In the transient region, the height can be seen to increase as $x^{\frac{1}{2}}$. In the recurrent region, it oscillates around a constant value. Fluctuations at recurrent occur due to randomised slope thresholds allowing for various stable heights. This behaviour is seen in Fig. 2, where it was plot to a shorter time for clarity.

The transient behaviour is considered as fractal, as changing system size displays the same distribution, thus being scale invariant. This is shown in Fig. 2 as zooming into smaller L shows the same behaviour at large L. Being a fractal indicates that the behaviours must follow a power law [2].

2a) Height against time, for small system sizes

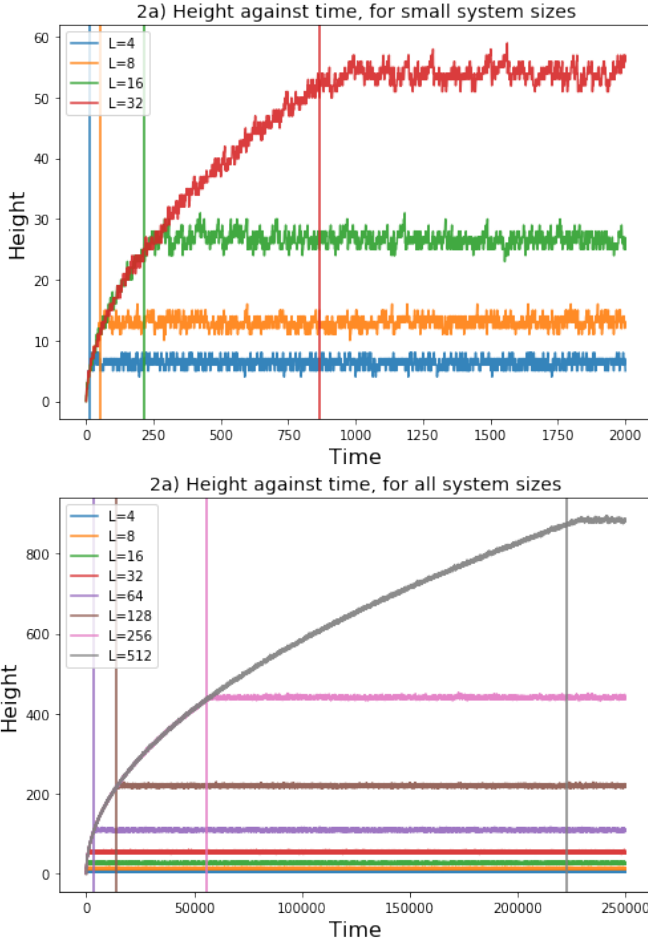

2a) Height against time, for all system sizes

Fig. 2. Heights of the pile were plotted at all times, to show height increasing by a power law in time when transient, and fluctuating around a constant value when recurrent. Solid vertical lines indicate the cross-over time. Different system sizes showing the same behaviour is characteristic of fractals, hence scale invariant **TOP**: shows system sizes up to $L = 32$, **BOTTOM**: shows all system sizes up to $L = 512$

2b) Cross-over time is the number of grains added before an additional grain added induces a grain to leave the system. It signifies a phase transition that changes the system behaviour. This was found numerically using a counter which stops counting after the first grain leaves. An average of 100 cross-overs were found. Plotting this relationship on a log scale shows average cross-over time $\langle t_C \rangle$ is quadratic against L to 3 s.f.

The log-log gradient was found for $L \geq 8$ to exclude boundary effects that arise from small system sizes, which skew the gradient value. This effect was only noticeable when analyzing corrections to scaling in Fig. 3.

Cross-over times were also verified by plotting their occurrence in height against time as vertical lines, found in Fig. 2.
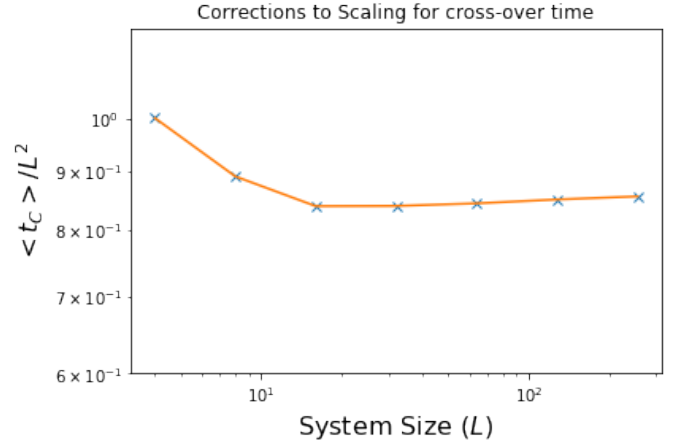

Fig. 3. Average cross-over time was corrected for scaling by dividing by L^2. Corrections were found to be required for $L \leq 8$. At large L, data points can be seen to increase compared to previous points. This was not expected, and is expected to be due to random thresholds.

2c) Considering the height of the pile $h(t; L)$ as

$$h(t; L) = \sum_{i=1}^{L} z_i(t) \tag{2}$$

where i is a site index. All slopes z_i can be approximated as an average value $\langle z \rangle$ as sites tend to an identical behaviour when $L \gg 1$. This reduces the equation to

$$h(t; L) = \sum_{i=1}^{L} \langle z \rangle$$
$$= L \cdot \langle z \rangle \tag{3}$$
$$\Rightarrow h(t; L) \propto L$$

showing that $h(t; L) \propto L$ for $L \gg 1$ where the average slope $\langle z \rangle$ tends to a constant.

Similarly for cross-over time $t_c(L)$, using the following relation

$$t_c(L) = \sum_{i=1}^{L} z_i \cdot i \tag{4}$$

cross-over time can be approximated by averaging all slopes to remove z_i from the sum. Applying the arithmetic sum formula $S_N = \frac{N(N+1)}{2}$,

$$t_c(L) = \langle z \rangle \cdot \sum_{i=1}^{L} i$$
$$= \langle z \rangle \cdot \frac{L(L+1)}{2} \approx \langle z \rangle \cdot L^2 \tag{5}$$
$$\Rightarrow t_c(L) \propto L^2$$

it is shown that cross-over time approximates as a quadratic relation when $L \gg 1$.

2d) Finite-size scaling analyzes how finite systems depend on its measured quantities, allowing critical exponents to be extracted, which could then be applied to represent an infinite system. Using Task 2b and 2c, an ansatz was be proposed as:

$$\tilde{h}(t;L) \propto \langle h \rangle \mathcal{F}\left(\frac{t}{\langle t_C \rangle}\right) \propto L^1 \mathcal{F}\left(\frac{t}{L^2}\right) \quad (6)$$

where $\tilde{h}$ is smoothed height over 10 realisations, $\mathcal{F}$ is the scaling function, *'something'* is $\langle h \rangle \sim L$ and *'argument'* is $\frac{t}{\langle t_C \rangle} \sim L^2$. Time is divided by the $\langle t_C \rangle$ to scale the transition from transient to recurrent to occur at the same time for all L. Dividing height by L finds the same average slope for all systems.

The behaviour of $\mathcal{F}(x)$ is expected to follow

$$\mathcal{F} \propto \begin{cases} \text{exponential increase} & \text{if } t \ll t_C \text{ (or } x \ll 1) \\ \text{constant} & \text{if } t \gg t_C \text{ (or } x \gg 1) \end{cases} \quad (7)$$

such that it describes the behaviour of both phases before and after cross-over. The data collapse is seen in Fig. 4.
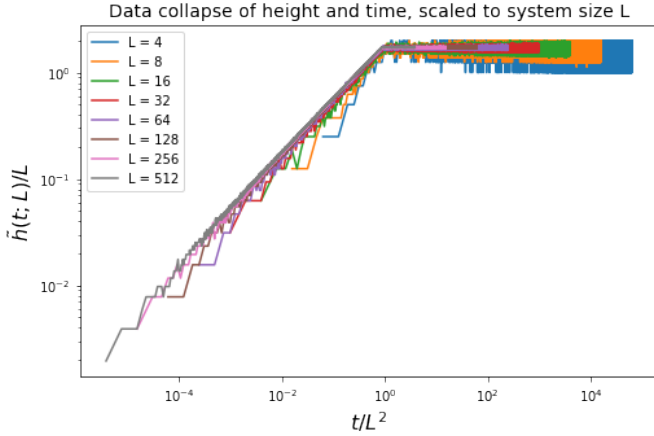

Fig. 4. Data collapse of smoothed height against time, scaled to their dependences on L. Scaling time causes transition from transient to recurrent to occur at same point. Scaling height finds the same average slope for all systems.

In the transient state, the slope of the line from Fig. 4 denotes the relationship of height to time. This was found as

$$h \propto t^{0.506} \quad (8)$$

where the slope of system $L = 512$ was used, as gradients in transient tended to 0.5 as $L \to \infty$ (demonstrated in code).

This relation was expected as Fig. 2 shows a power law with a positive exponent less than one. A second data collapse with this exponent was performed by scaling height with time, and is seen in Fig. 5 indicating these exponent values as characteristic. The collapse could be improved by taking plots of $L \geq 256$.

In the transient state, the ratio of height to time remains around one. In the recurrent state, the height to time ratio decreases as height remains roughly constant while time increases.
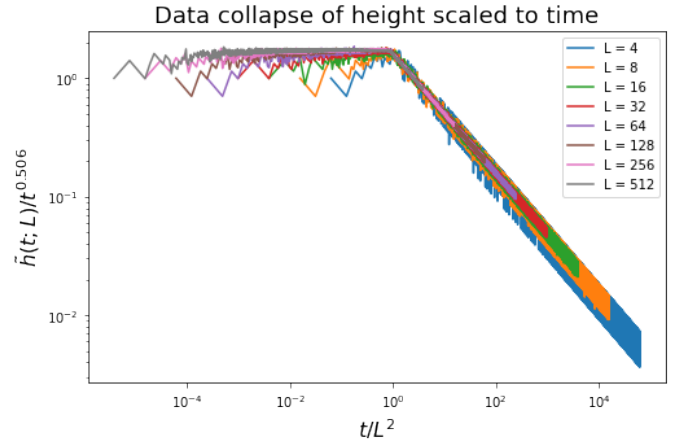

Fig. 5. Data collapse of smoothed height against time, scaled to time and system size respectively. Ratio of height to time remains around one in transient. Height to time ratio decreases as height remains roughly constant while time increases in recurrent.

2e) Corrections to scaling are required as $\langle z \rangle$ for small L was much lesser than $\langle z \rangle$ for large L. Corrections were assumed to take the form of

$$\langle h(t;L) \rangle_t = a_0 L \left(1 - a_1 L^{-\omega_1} + a_2 L^{-\omega_2} + \dots\right) \quad (9)$$

where $\langle h(t;L) \rangle_t$ is average height, and a_i, ω_i are constants of scaling. Only a_0 and ω_1 were determined. At large L, average height $\langle h(t;L) \rangle_t$ tends to $a_o L$ as the remaining correction $L^{-\omega_i}$ terms tends to zero as they are to the power of a negative exponent since $\omega_i > 0$. This gives a way to estimate the value of a_0, as $\frac{\langle h(t;L) \rangle_t}{L} \sim a_0$.

To estimate ω_1 higher order terms were ignored, and the scaling relation is found as

$$\langle h(t;L) \rangle_t = a_0 L \left(1 - a_1 L^{-\omega_1}\right)$$
$$\frac{\langle h(t;L) \rangle_t}{a_0 L} = 1 - a_1 L^{-\omega_1} \quad (10)$$
$$\log\left[1 - \frac{\langle h(t;L) \rangle_t}{a_0 L}\right] = -\omega_1 \log L + \log a_1$$

where the final form is a straight line fit on a log-log plot, with its negative gradient gives ω_1.

A chi-square χ^2 minimisation was implemented to obtain the value for a_0. Chi-square is given by

$$\chi^2 = \sum_i \frac{(O_i - E_i)^2}{E_i} \quad (11)$$

where O_i is the observed value and E_i is the expected value. In this case, O is the value obtained by Eqn. 10 for a given a_0 value at a certain L, and E is the expected value for a given L applied to a straight line fit between the first and last point using Eqn. 10. In essence, χ^2 measured how far the values strayed from a straight line. This minimisation is shown in Fig. 6.

Values of a_0 in the range of $[1.72, 1.8]$ at an interval of 10^{-6} were tested. This produced the following values:

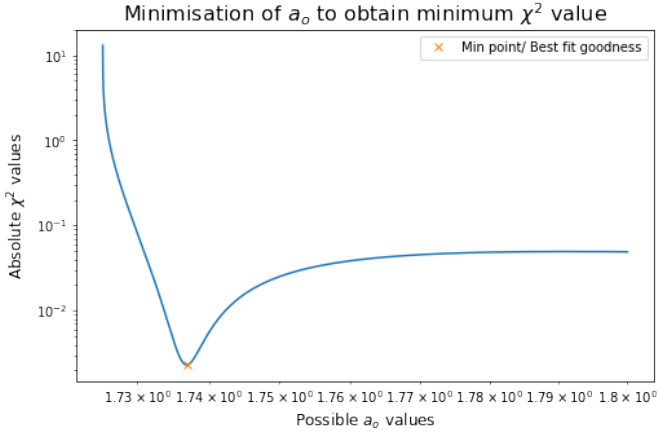- $a_0 = 1.737$
- $\omega_1 = 0.548$

Fig. 6.   Chi-square minimisation was used to find the value of a_0 which provided the straightest line of best fit between the initial and final points. A clear minimum point can be seen from the plot, this was found as $a_0 = 1.737$.

Applying these terms to Eqn. 22, the effect of additional correction terms can be seen in Fig. 7. An oscillatory behaviour over an amplitude range of 0.03, indicates a minimal effect to scaling of h.
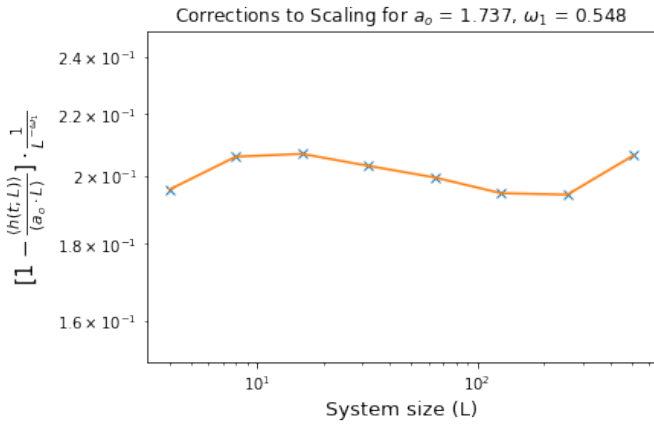

Fig. 7.   Plot to observe effect of additional correction constants to scaling corrections. Shows an oscillatory behaviour over an amplitude range of 0.03, and thus roughly horizontal. This indicates a minimal effect on height h

2f) Standard deviation of height σ_h was found to scale with system size as:

$$\sigma_h \propto L^{0.253} \tag{12}$$

where this was derived from the log-log gradient of σ_h against L. The expected exponent is ~ 0.24 [3]. No corrections to scaling were found for σ_h as seen in Fig. 8, indicating Eqn. 12 to apply at all L.

Since the average slope is $\langle z \rangle = \frac{\langle h \rangle}{L}$, the corrections to scaling for $\langle h \rangle$ from Eqn. 22 can be expressed as

$$\frac{\langle h(t; L) \rangle}{L} = a_0 \left(1 - a_1 L^{-\omega_1} + a_2 L^{-\omega_2} + \ldots \right) \tag{13}$$

$$\langle z \rangle \approx a_0 \text{ (as } L \gg 1)$$

where the correction terms to negative exponents tend to zero for large L, and thus average slope $\langle z \rangle$ tends to a_0. Since $\langle z \rangle$ tends a constant, its standard deviation $\sigma_{\langle z \rangle}$ will tend to zero.
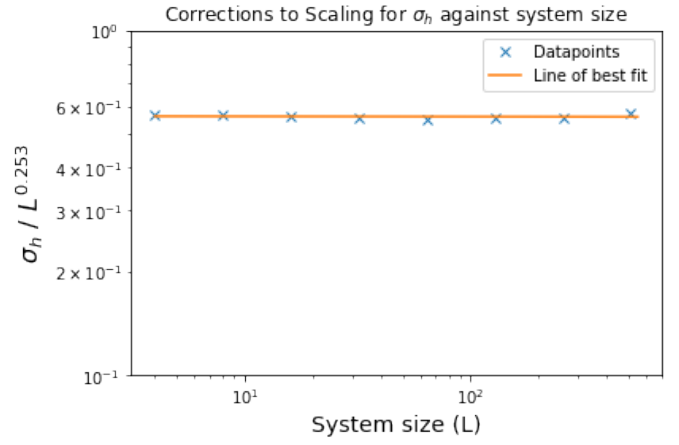

Fig. 8.   Scaling corrections for σ_h, by dividing by dependence on L. Data points show a straight horizontal line, indicating no requirement scaling corrections, indicating the relationship to apply at all L. $L^{0.253}$ was found by analysing the gradient of a straight line fit on a log-log plot, using a least squares fit.

2g) Assuming identical, independently distributed variables, these random variables will tend to a normal distribution following the Central Limit Theorem (CLT) after a large number of samples have been taken. We expect this for $L \gg 1$ where boundary effects are negligible. Note, that original variables need not be normally distributed in the CLT [4].

To test this, the distribution of probability to height was investigated, giving Gaussian-like distributions of different heights for each L. Assuming a perfect Gaussian of form

$$P(h; L) = \frac{1}{\sigma_h \sqrt{2\pi}} \exp \left[-\frac{1}{2} \left(\frac{h - \langle h \rangle}{\sigma_h} \right)^2 \right] \tag{14}$$

where $P(h; L)$ is the probability of a height, a collapse was performed. $P(h; L)$ and h were adjusted as

- $h \Rightarrow \frac{h - \langle h \rangle}{\sigma_h}$
- $P(h; L) \Rightarrow P(h; L) \cdot \sigma_h$

normalising the dependence of both variables from variables that depend on L. Fig. 9 shows the collapse.

To find how σ_h scales with height, consider its relationship to the standard deviation of the average slope $\sigma_{\langle z \rangle}$ from Eqn. 13,

$$\sigma_h = \sigma_{\langle z \rangle} \cdot L \tag{15}$$

where it should be noted again that σ_h is for average height.

Since the average slope is found from L sites, or L measurements, σ_z is analogous to the standard error on the mean for $\langle z \rangle$, for n samples using CLT. Thus is written as

$$\sigma_{\langle z \rangle} = \frac{\sigma}{\sqrt{n}} = \frac{\sigma}{\sqrt{L}} \tag{16}$$

where σ is the standard deviation of average slope not considering multiple measurements.

Combining Eqn. 15 and 16, this gives the relationship,

$$\sigma_h = \sigma_{\langle z \rangle} \cdot L = \sigma \cdot L^{1-0.5}$$
$$\Rightarrow \sigma_h \propto L^{0.5} \tag{17}$$

disagreeing to the relationship found from **2f)**.
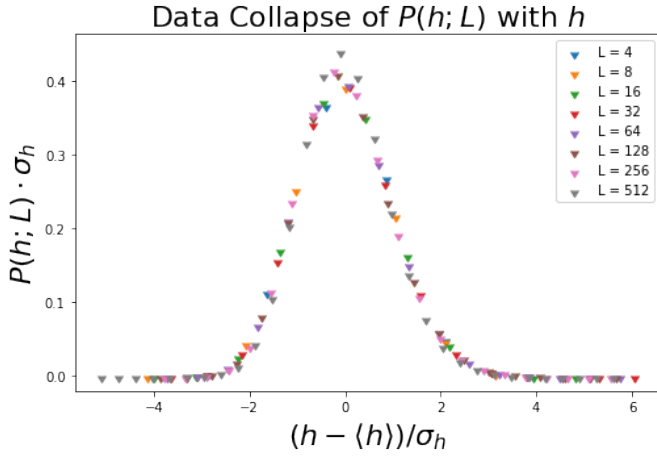
Data Collapse of $P(h;L)$ with h

Fig. 9. Data collapse of height probability to height. Distribution shows a Gaussian-like shape, however is not a true Gaussian as sites are not independent. Sites will always have an influence on neighbouring sites, at any system size.

This implies that the distribution is not a true Gaussian, hence the variables are either not identical, or not independent.

The skewness of Fig. 9 was found as $S = 0.0294$, using the Fisher-Pearson Coefficient [5]. This is expected to be zero for a Gaussian, reinforcing it as non-Gaussian. This skew was due to slopes far from $i = 1$ toppling less frequently.

For $L \gg 1$, all sites *do* tend to being identical, as average slope values tend to the same value $\langle z \rangle \sim 1.75$. Only near boundaries are the sites not identical, but this effect will be negligible as $L \to \infty$ (distribution of slope values seen in code).

Consider correlation length as the range of effect that a site has on other sites. At small system sizes, the effect of a boundary on all sites will be large, greatly influencing z_i values. At large system sizes, this effect reduces, only affecting sites close to the boundary. Thus, we see that this effect is roughly constant for any system size, as it only reaches sites close to the boundary.

However this is not localised to boundary effects, individual sites will also have an effect on neighbouring sites, that will also be constant at any L.

Therefore, it can be said that the correlation length of any site on neighbouring sites will be constant at all system sizes. This implies that a site will always influence its neighbouring sites, and that z_i will *never* be independent even if $L \to \infty$.

Gaussian-like distributions are often seen for 'weak-interacting' systems like this one, i.e. systems where sites only have a short range dependence on other sites.

C. Avalanche-size Probability $P(s;L)$

3a) Log-binning is a technique used to extract information when the statistics are insufficient to describe true behaviour. It reduces the number of samples taken to display the same characteristics, increasing computational efficiency.

Probability and log-binned probability against avalanche size s can be seen in Fig. 10. The log-binning was done using 'logbin230119.py' [6]. When adjusting the scale, a
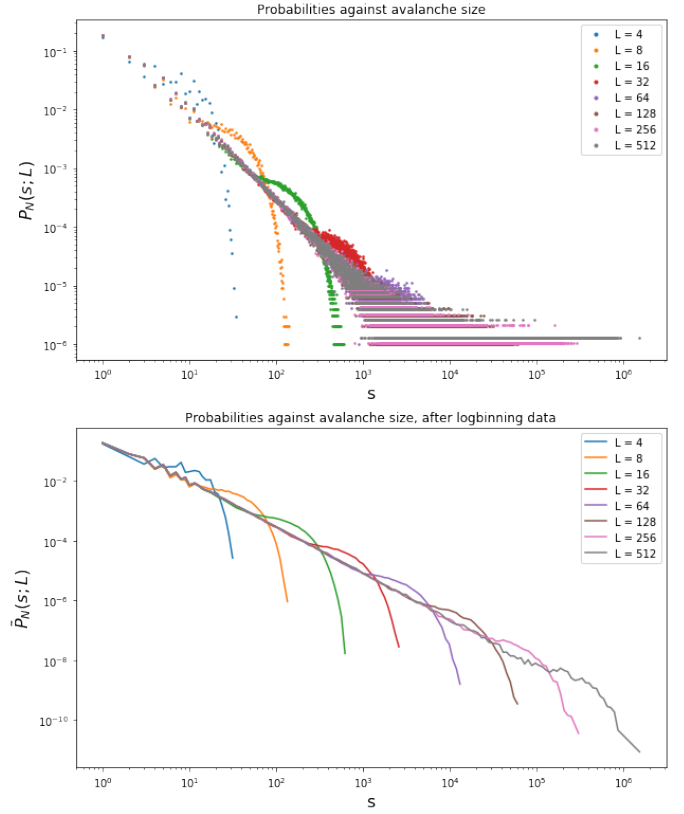

Fig. 10. **TOP:** Probability of avalanche size against avalanche size, found by using 'logbin230119.py' but scale set to 1. **BOTTOM**: Log-binned data using scale - 1.1, shows a smoother plot that better described characteristics of ricepile. For $L = 256, 512$, $\tilde{P}(s;L)$ is not as smooth as distributions for smaller L, as log-binning scale is not large enough to encompass larger avalanche sizes.

compromise between smoothness and bin-size must be found. Having a large bin-size increases the interval that points may lie, increasing smoothness but also causing a loss of information in the location of points. A scale of 1.1 was used. There is no direct correspondence between $P(s;L)$ and $\tilde{P}(s;L)$, but both represent equivalent quantities. Avalanches of size zero were not included in the plot, but $\tilde{P}(s;L)$ are normalised using $s = 0$ values.

For each L, a bump is seen at certain avalanche sizes. This is because a finite sized system is used. Avalanche sizes that could reach larger values are cut off early as a grain leaves the system, leading to an excess of certain s values. This explains why the bumps don't overlap. In an infinite system, $\tilde{P}(s;L)$ against s would be a straight line of negative gradient on a log-log scale (power-law decay). Avalanche sizes much larger than system size were also noticed for each L.

For $L \geq 8$, "zig-zaging" can be seen from small avalanche sizes. Odd avalanches are slightly favoured compared to even avalanches, up to $s \sim 13$ and excluding $s = 1$. As one grain topples, its threshold re-generates and it affects two neighbouring sites. Those two affect another one, two or three sites. However since $z = 2$ is more likely, only the outer two are likely to have a slope ready to topple, whereas the inner slope/ original site is now likely to be within threshold, causing an avalanche size of 3. This argument then applies for slightly

larger avalanche sizes, favouring odd. For $s \gg 1$, subsequent sites that cause topplings reduces this effect, removing the odd avalanche favorability. Transition probabilities for small systems can be calculated [7]. $L = 4$ doesn't act in this way due to strong boundary effects.

For $L = 256, 512$, $\tilde{P}(s; L)$ is not as smooth as distributions for smaller L. This is because the log-binning scale is not large enough to encompass larger avalanche sizes.

3b) $P_N(s; L)$ agrees with the finite-size scaling ansatz,

$$\tilde{P}_N(s; L) \propto s^{-\tau_s} \mathcal{G}\left(s/L^D\right) \qquad (18)$$

as seen in Fig. 11 for $L \gg 1$ and $s \gg 1$.

Taking $L \geq 16$ and $s \geq 13$ improved the data collapse. Critical exponents were estimated as $D = 2.20$ and $\tau_s = 1.55$, qualitatively by eye.
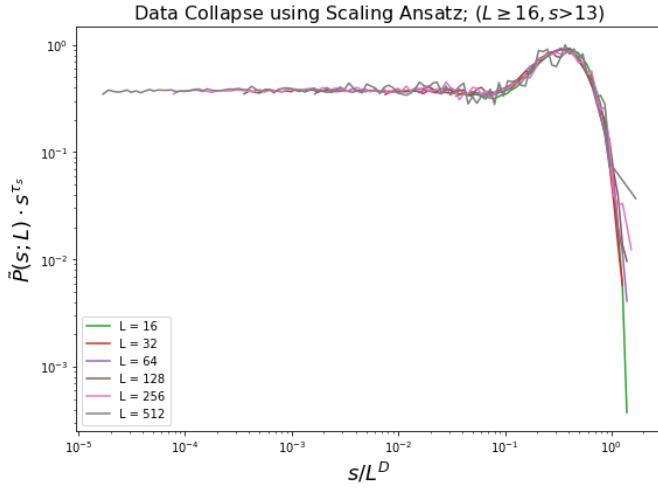

Fig. 11. Data collapse of avalanche size probability and avalanche size. Collapse for $L \geq 16$ and $s \geq 13$. This removes boundary effects and the effect described in **3a)** of zig-zaging. By eye, data collapse appears to be aligned well for L values used.

3c) Avalanche moments are derived as:

$$\left\langle s^k \right\rangle = \lim_{T \to \infty} \frac{1}{T} \sum_{t=t_0+1}^{t_0+T} s_t^k = \sum_{s=1}^{\infty} s^k P(s; L) \qquad (19)$$

where k is an integer value [6]. Moments can be used to estimate avalanche size probability $P(s; L)$ from fewer calculations, and to estimate the critical exponents D and τ_s. The k'th moment $\left\langle s^k \right\rangle$ scales as a power law with L, seen in Fig. 12.

To find D and τ_s for $L \gg 1$, the finite-size scaling ansatz in Eqn. 18 was combined with $\left\langle s^k \right\rangle$ to develop a prediction to scaling

$$\left\langle s^k \right\rangle \propto L^{D(1+k-\tau_s)}$$
$$\log\left\langle s^k \right\rangle \propto D\left(1 + k - \tau_s\right) \log L \qquad (20)$$

where $(1 + k - \tau_s) > 0$, a sum to integral approximation was done, and the gradient is $f(k) = D\left(1 + k - \tau_s\right)$ [1]. Four moments $k = [1, 2, 3, 4]$ were plotted, giving four values for $f(k)$. This can be rearranged as

$$f(k) = D(1 + k - \tau_s)$$
$$= Dk + D(1 - \tau_s) \qquad (21)$$

such that a straight line fit of $f(k)$ against k on provides D as the slope, and τ_s from the y-intercept. The exponent depends only k, as seen in Fig. 13, verifying the prediction to scaling.

Critical Exponents were found as

- $D = 2.2149$
- $\tau_s = 1.5549$

where it is expected that the values are not ideal as the system sizes tested are insufficiently large.
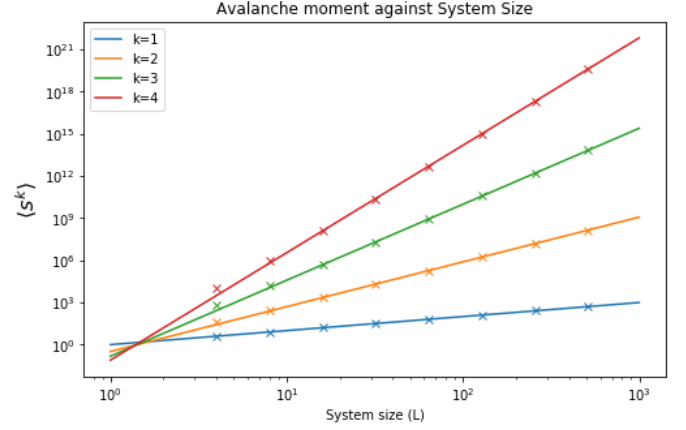

Fig. 12. Avalanche size to the k'th moment against system size. Small L for $k > 1$ seen to require corrections to scaling as do not fit onto straight line fit. The gradient of each moment can be used to estimate D and τ_s
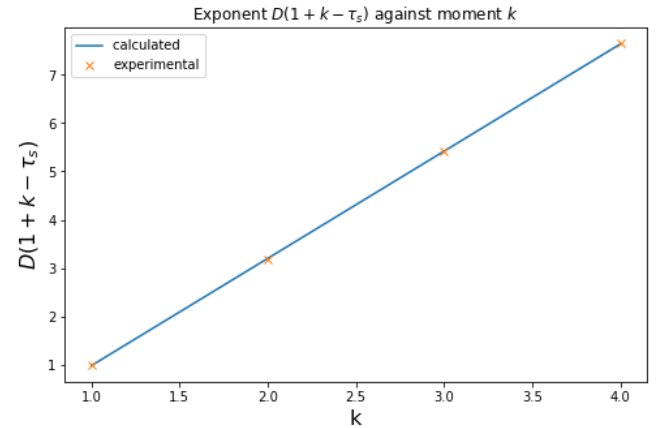

Fig. 13. Avalanche size scaling exponents and their dependence of k. Shows that scaling with L only depends on k, where D and τ_s are true constants.

From Fig. 12, values of small $L < 8$ appeared not fit onto the straight line fit due to corrections to scaling. To verify this, $\left\langle s^k \right\rangle$ was divided by its dependence on L, where a straight line is to be expected if no scaling corrections are necessary, equaling to a constant. This is seen in Fig. 14, where it shows that only the 1st moment requires no corrections and subsequent moments do. Addtionally, this implies that the average avalanche size for all system sizes are the same.

A similar form of corrections to scaling was used, such that

$$\left\langle s^k \right\rangle = b_0 L^{D(1+k-\tau_s)}\left(1 - b_1 L^{-\gamma_1} + b_2 L^{-\gamma_2} + \ldots\right) \qquad (22)$$

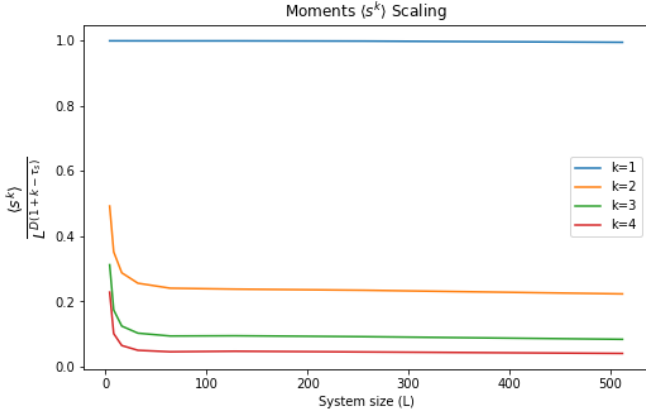where b_0 and γ_1 were found following the same method in **2e)**. The following relationship

Fig. 14. $\langle s^k \rangle$ divided by dependence of L to demonstrate corrections to scaling. It is seen that only moments $k > 1$ require corrections.

$$\log\left[\frac{\langle s^k \rangle}{L^{D(1+k-\tau_s)}} \cdot \frac{1}{b_0} - 1\right] = -\gamma_1 \log L + \log a_1 \quad (23)$$

was plot against L to find γ_1 and is seen in Fig. 15.
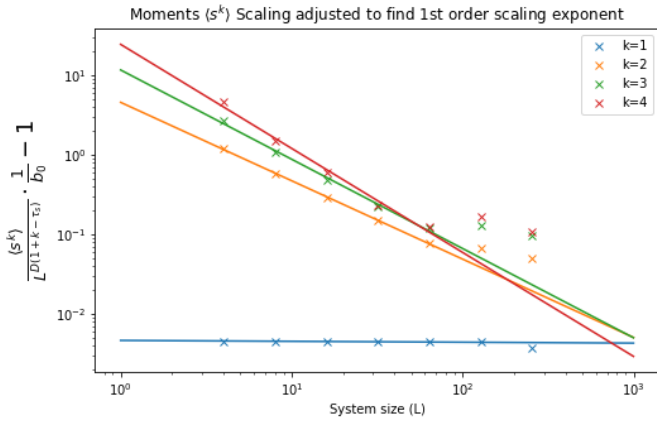

Fig. 15. Avalanche size moment was adjusted to discover the 1st order correction scaling exponent γ_1 to L as in Eqn. 23. $L = 256, 512$ seen to plateau, indicating minimal effect to corrections to scaling, hence was ignored in finding γ_1

For $L \geq 256$, values can be seen to plateau in Fig. 15, this was thought to be due to a reduction in the effect of corrections to scaling. Therefore, these points were ignored when finding γ_1. This analysis yielded the following values

- (k=1) $b_0 = 0.995$, $\gamma_1 = 0.011$
- (k=2) $b_0 = 0.223$, $\gamma_1 = 0.987$
- (k=3) $b_0 = 0.084$, $\gamma_1 = 1.124$
- (k=4) $b_0 = 0.041$, $\gamma_1 = 1.310$

Relationships between γ_1 and b_0 with k described a power law relationship that approximates to $\gamma_1 \sim k^{0.5}$ and $b_0 \sim k^{-2}$. However, these relationships could not be collapsed onto a straight line in log-log, indicating dependence on additional variables. More analysis could be done to discover these dependencies.

III. CONCLUSION

Aim of this project was to analyse the Oslo model of a ricepile, to investigate a self-organised critical system. Main achievements in understanding include: observing fractal behaviour leading to scale invariance, applying finite-sized scaling ansatzs and data collapses to extract relationships between quantities, investigating corrections to scaling due to finite-sized systems, log-binning to extract behaviours efficiently, discovering Gaussian-like nature of weak-interacting systems, and applying moments to extract critical exponents in avalanche sizes.

REFERENCES

[1] K. Christensen, N.R. Moloney. Complexity and Criticality. Imperial College Press Advanced Physics Texts. 2005.
[2] D. Lee. Statistical Mechanics Course Notes. Imperial College London. 2020.
[3] A. Corral and M. Paczuski, Phys. Rev. Lett. 83, 572. 1999
[4] M. Rouaud. Probability, Statistics and Estimation. p. 10. 2013
[5] NIST Handbook. Measures of Skewness and Kurtosis. *https://www.itl.nist.gov/div898/handbook/eda/section3/eda35b.htm*. Accessed on 14th February 2020.
[6] K. Christensen. Complexity Project Notes, Complexity and Networks Course. 2020
[7] A. Corral. Calculation of the transition matrix and of the occupation probabilities for the states of the Oslo sandpile model. Physical Review E. 2004